Organic Electronics 30 (2016) 265–274

Contents lists available at ScienceDirect

Organic Electronics

journal homepage: www.elsevier.com/locate/orgel

Bipolar transport materials for electroluminescence applications

Yi-Wei Tsai [a, b], Jen-Shyang Ni [a], Feng-Ling Wu [a], Ming-Chang P. Yeh [b, **], Yu-Jen Cheng [a], Li-Zhong Tsai [c], Siao-Yin Yu [c], San-Yu Ting [c], Li-Yin Chen [c, ***], Yuh Sheng Wen [a], Mandy M. Lee [a], Jiann T. Lin [a, *]

[a] Institute of Chemistry, Academia Sinica, Taipei 11529, Taiwan
[b] Department of Chemistry, National Taiwan Normal University, Taipei, Taiwan
[c] Department of Photonics, National Sun Yat-sen University, Kaohsiung 804, Taiwan

ARTICLE INFO

Article history:
Received 18 September 2015
Received in revised form
23 December 2015
Accepted 24 December 2015
Available online 8 January 2016

Keywords:
Organic light emitting diode
Ambipolar
Wide band gap
Flurorescence emitter
2,3-benzofuran

ABSTRACT

Benzofuranyl benzene incorporating naphthyl (phenothiazinyl or dimesitylboryl) entities via meta-conjugation have been synthesized. These compounds exhibit bipolar transport characteristic with mobilities in the range of 10^{-5} to 10^{-4} cm^2/V s at an electric field of 4×10^5 V/cm. The compounds with two naphthyl or dimesitylboryl substituents emit in the violet region with good solution quantum yields. The OLEDs fabricated from the benzofuranyl/dimethylboryl, benzofuranyl/naphthyl and benzofuranyl/dimethylboryl/phenathiazine derivatives have maximum external efficiencies of 1.01%, 1.41% and 3.14%, respectively.

1. Introduction

Organic light-emitting diodes (OLEDs) continue to be of great interest because of high potential in lighting and display technology. Emitting materials with larger HOMO/LUMO gap, such as blue- or violet emitters, are important for several reasons: (1) they can be used for the prime color of their own in all color display; (2) they can be used as the energy transfer donor for different color emission; (3) violet or blue light laser is useful for information technology. An important component used in OLEDs is the host material for emitting guests, especially when expensive phosphorescent metal complexes are used as the guest. Though bipolar transport is not prerequisite for an emitter, emitters of the type may have some advantages: (1) dispensation with additional hole and electron transport materials is possible; (2) they help with carrying electron and holes to the emitters when used as the host.

In order to have a larger HOMO/LUMO gap, a compound with extended conjugation should be avoided. Electronic coupling through a *meta*-phenylene bridge (*m*-Ph) is generally weaker than through a *para*-phenylene (*p*-Ph) bridge [1] even though the difference becomes smaller at the excited state [2]. An easy approach for a material to be able to transport electrons and holes is to incorporate entities capable of electron- (ET) and hole-transporting (HT) at the same molecule, though the number of ET and HT entities, and the linkage between them will also affect the overall carrier mobility [3]. We have been interested in bipolar transport materials as the emitter or the host for phosphorescent OLEDs. In addition to be a host, we found these materials may also be used as single-layer OLEDs if they are emitting [4]. Our interest in the materials with large HOMO/LUMO gap leads us to construct *m*-Ph derivatives containing both potential ET and HT entities at mutual *meta*-sites. Benzofuran entity was selected as one of our HT candidates due to the high tendency of benzofuran derivatives to emit in the blue region [5]. Another possible HT candidate is *N*-conjugated 10*H*-phenothiazine entity, an electron donor which can provide large HOMO/LUMO gap when linked to an acceptor via a *m*-Ph unit [6]. For the ET entity, a stable electron deficient dimesitylboryl entity [7], known to be beneficial to electron transport [8] and light emission [9] when incorporated in the conjugated molecules, was chosen. In this paper we will report new *m*-Ph

* Corresponding author.
** Corresponding author.
*** Corresponding author.
E-mail addresses: cheyeh@scc.ntnu.edu.tw (M.-C.P. Yeh), ly_chen@mail.nsysu.edu.tw (L.-Y. Chen), jtlin@gate.sinica.edu.tw (J.T. Lin).

http://dx.doi.org/10.1016/j.orgel.2015.12.026
1566-1199/

derivatives capable of bipolar transport and relevant physical properties including X-ray crystal structures analyses of some compounds.

2. Experimental section

2.1. General information

Unless otherwise specified, all the reactions were carried out under nitrogen atmosphere using standard Schlenk techniques, and the solvents used were purified by standard procedures. All column chromatography was performed with the use of silica gel (230–400 mesh, Macherey–Nagel GmbH & Co.) as stationary phase. The ^{1}H NMR spectra were recorded on a Bruker AMX400 spectrometer. Electronic absorption spectra were measured in dichloromethane using a Cary 50 Probe UV–visible spectrophotometer. Emission spectra were recorded by a Hitachi F-4500 spectrofluorometer. Emission quantum yields were measured in organic solvents by standard methods [10] with reference to quinine sulfate dehydrate in H_2O (Φ = 0.56) [10b] or 9,10-diphenylanthracene in cyclohexane (1.0×10^{-5} M, Φ = 0.97). Cyclic voltammetry experiments were performed with a CHI–621B electrochemical analyzer. All measurements were carried out at room temperature with a conventional three-electrode configuration consisting of platinum working and auxiliary electrodes and a nonaqueous $Ag/AgNO_3$ reference electrode. The $E_{1/2}$ values were determined as $1/2(E_p^a + E_p^c)$, where E_p^a and E_p^c were the anodic and cathodic peak potentials, respectively. The solvent in all experiments was CH_2Cl_2 and the supporting electrolyte was 0.1 M tetrabutylammonium perchlorate. DSC measurements were carried out using a Perkin–Elmer 7 series thermal analyzer at a heating rate of 10 °C/min. TGA measurements were performed on a Perkin–Elmer TGA7 thermal analyzer. FAB-mass spectra were collected on a JMS-700 double focusing mass spectrometer (JEOL, Tokyo, Japan) with a resolution of 8000 (5% valley definition). For FAB-mass spectra, the source accelerating voltage was operated at 10 kV with a Xe gun, using 3-nitrobenzyl alcohol as the matrix. Elementary analyses were performed on a Perkin–Elmer 2400 CHN analyzer. Low-energy photoelectron spectra were taken from a photoelectron spectrometer (AC-2, Riken-Keiki PT5-0210).

2.2. Synthesis

2.2.1. Benzofuran-2-yltributylstannane (**1a**)

To a flask containing benzofuran (1.00 g, 84.6 mmol) in THF (85 mL) prechilled to −78 °C was added *n*-BuLi (1.6 M in hexane, 3.17 mL, 5.07 mmol) dropwise, and the solution changed color from bright yellow to light orange. After the solution was stirred for 1 h at the same temperature, Bu_3SnCl (2.42 mL, 8.88 mmol) was injected and the solution turned into light brown color. The solution was warmed to room temperature and stirred for 18 h. Aqueous KF was added to quenched the excess Bu_3SnCl, and the mixture was extracted with Et_2O/saturated aqueous NH_4Cl for several times. The collected organic extracts were dehydrated by anhydrous $MgSO_4$ and filtered through Celite. The filtrate was pumped dry and the residue was ourified by column chromatography using hexanes as the eluent. The compound **1a** was isolated as light yellow oil in 99% yield (3.44 g).

2.2.2. 2-(3,5-Dibromophenyl)benzofuran (**1b**)

DMF (0.5 M, 25 mL) was added to a flask loaded with 1,3,5-tribromobenzene (11.6 g, 36.9 mmol), **1a** (5.0 g, 12.3 mmol) and $PdCl_2(PPh_3)_2$ (0.26 g, 0.369 mmol), and the dark brown solution was stirred at 80 °C for 1 day. After removal of the solvent, the residue was dissolved in CH_2Cl_2 and treated with aqueous KF to quench **1a**. The mixture was extracted with Et_2O/saturated aqueous NH_4Cl for several times. The collected organic extracts were dehydrated by anhydrous $MgSO_4$ and filtered through Celite. The filtrate was pumped dry and the residue was ourified by column chromatography using hexanes as the eluent. The compound **1b** was isolated as a white powder in 49% yield. ^{1}H NMR (acetone-d_6, 400 MHz): δ 8.11 (br, 2H), 7.77 (s, 1H), 7.69 (d, J = 7.6 Hz, 1H), 7.62 (d, J = 8.4 Hz, 1H), 7.55 (s, 1H), 7.39 (pseudo triplet, 1H), 7.30 (pseudo triplet, 1H). ^{13}C NMR (acetone-d_6, 125 MHz): δ 156.1, 153.3, 135.1, 134.4, 129.9, 127.4, 126.5, 124.5, 122.6, 112.2, 105.4. HRMS (FAB, *m*/*z*): [M^+] calcd for $C_{14}H_8Br_2O$: 349.8942; found: 348.8948.

2.2.3. 2-(3,5-Di(naphthalene-1-yl)phenyl)benzofuran (**C-naOL**)

To a flask loaded with **1b** (2.24 g, 6.37 mmol), naphthalene-1-ylboronic acid (3.28 g, 19.1 mmol), Na_2CO_3 (2.02 g, 19.1 mmol) and $Pd(PPh_3)_4$ (0.37 g, 0.319 mmol) was added toluene (22 mL). Water (10 mL) and ethanol (5.0 mL) were then added and the solution was heated at 80 °C for 18 h. After removal of the solvent, the residue was dissolved in CH_2Cl_2 and filtered through Celite. The filtrate was extracted with CH_2Cl_2/saturated aqueous NH_4Cl for several times. The collected organic extracts were dehydrated by anhydrous $MgSO_4$ and filtered. The filtrate was pumped dry and the residue was further purified by column chromatography using hexanes as the eluent. The crude product was recrystallized from CH_2Cl_2/MeOH to provide **C-naOL** as a white powder in 80% yield (2.27 g). ^{1}H NMR (chloroform-d_1, 500 MHz): δ 8.14 (d, J = 7.6 Hz, 2H), 8.13 (s, 2H), 7.96 (dd, J = 6.8; 1.2 Hz, 2H), 7.93 (d, J = 6.0 Hz, 2H), 7.68 (s, 1H), 7.62–7.57 (m, 5H),7.56–7.50 (m, 5H),7.30 (td, J = 6.4; 1.0 Hz, 1H),7.25 (t, J = 6.0 Hz, 1H),7.11 (s, 1H). ^{13}C NMR (chloroform-d_1, 125 MHz): δ 155.9, 155.2, 141.7, 139.7, 134.1, 132.1, 131.8, 130.9, 129.4, 128.6, 128.3, 127.3, 126.5, 126.1, 126.1, 125.7, 125.6, 124.7, 123.2, 121.2, 111.4, 102.2. HRMS (FAB, *m*/*z*): [M^+] calcd for $C_{34}H_{22}O$: 446.1671; found: 446.1688. Anal Calcd for $C_{34}H_{22}O$: C, 91.45; H, 4.97. Found: C, 91.17; H, 5.13.

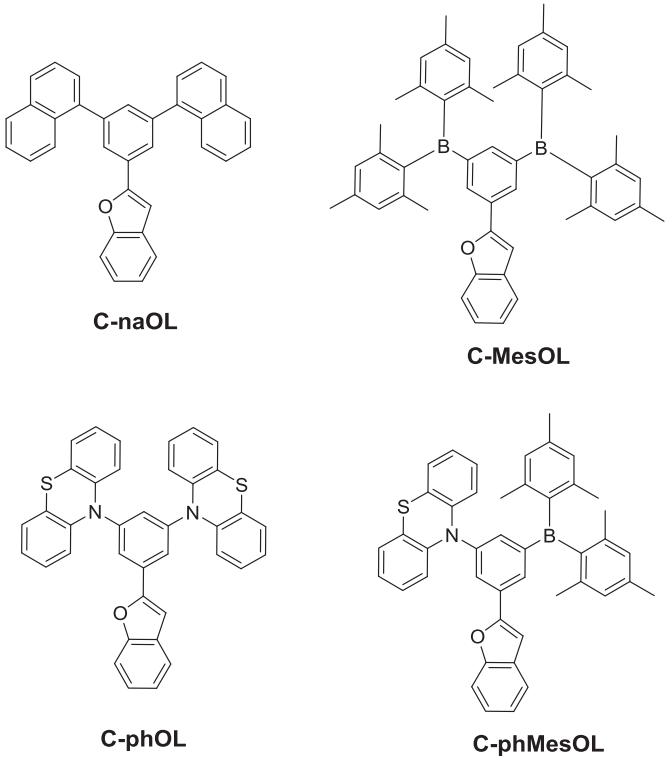

Fig. 1. Molecular structures of the compounds.

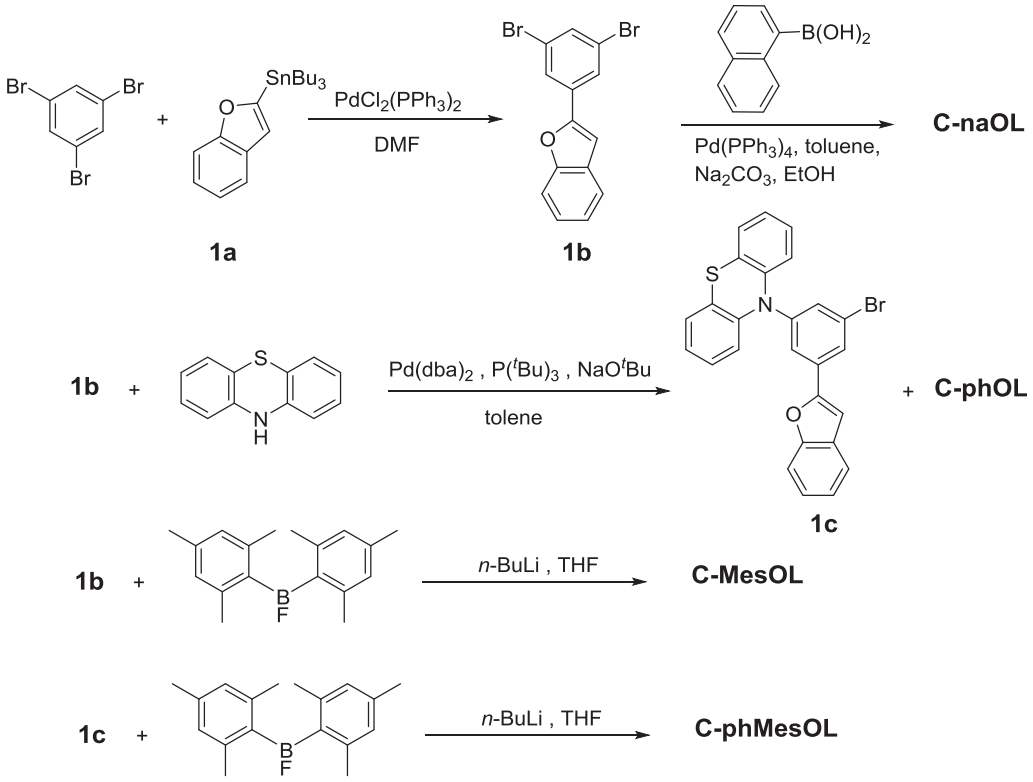

Scheme 1. Synthetic routes of the compounds.

Table 1
Physical properties of the compounds.

cpd	λ_{abs},[a] nm	λ_{em},[b] nm	Φ[c]	E_{ox} (ΔE_p)[d] mV	HOMO/LUMO,[e] eV	$E_{0\text{-}0}$,[f] eV	$T_g/T_m/T_c/T_d$,[g] °C
C-naOL	308	355	0.80	1010 (i)	−5.51 (−5.99)/-1.30	3.79 (3.78)	78/193/nd/319
C-MesOL	308	416	0.33	1030 (i)	−5.48 (−6.03)/-1.74	3.24 (3.29)	110/254/nd/255
C-phOL	310	508	nd	292 (99), 462 (86)	−5.04 (−5.44)/-1.68	2.57 (2.80)	105/247/188/338
C-phMesOL	308	416, 596	nd	292 (96)	−4.88 (−5.47)/-1.90	2.22 (2.46)	103/235/nd/293

[a] Recorded in CH_2Cl_2 at 298 K.
[b] Recorded in toluene solutions.
[c] Reference for **C-naOL**: 1.0×10^{-5} M Quinine sulfate dehydrate in 0.05 M $H_2SO_{4(aq)}$ ($\Phi = 0.56$); for **C-MesOL**: 9,10-diphenylanthracene in cyclohexane (1.0×10^{-5} M, $\Phi = 0.97$).
[d] Measured in CH_2Cl_2. i: irreversible wave. For **C-naOL** and **C-MesOL**, E_{ox} was recorded at the onset point. For **C-phOL** and **C-phMesOL**, $E_{ox} = 1/2(E_{pa} + E_{pc})$, $\Delta E_p = E_{pa} - E_{pc}$ where E_{pa} and E_{pc} are anodic and cathodic potentials, respectively. All the potentials are reported relative to ferrocene, which was used as the internal standard in each experiment.
[e] The HOMO energies were obtained from theoretical computation, or measured by a low-energy photoelectron spectrometer (in parenthesis), and the LUMO energies were obtained from the computation.
[f] HOMO/LUMO gap was calculated by the onset of emission absorption spectra and from computation (in parenthesis).
[g] T_g: glass transition temperature, T_m: melting point, T_c: crystallization point, T_d: decomposition temperature taken at 5% weight loss. nd: not detected.

2.2.4. (5-Benzofuran-2-yl)-1,3-phenylene)bis(dimesitylborane) (*C-MesOL*)

The flask containing a THF solution (10 mL) of **1b** (2.55 g, 7.24 mmol) was cooled to −78 °C. *n*-BuLi (2.5 M in hexane, 8.70 mL, 21.7 mmol) was added slowly, and the solution turned into dark red color. After being stirred for 45 min at the same temperature, a THF solution (10 mL) of dimesityl boronfluoride (4.95 g, 22.4 mmol) was added. The solution was slowly warmed to room temperature and stirred for 18 h. After removal of THF by a rotary evaporator, the solution was extracted with CH_2Cl_2/saturated aqueous NH_4Cl for several times. The collected organic extracts were dehydrated by anhydrous $MgSO_4$ and filtered. The filtrate was pumped dry and the residue was further purified by column chromatography using hexanes as the eluent. The residue was further purified by column chromatography using hexanes as the eluent. The crude product was recrystallized from CH_2Cl_2/MeOH to provide **C-MesOL** as a white powder in 15% yield (0.60 g). ^{1}H NMR (acetone-d_6, 400 MHz): δ 8.13 (s, 2H), 7.60 (d, J = 8.0 Hz, 1H), 7.58 (s, 1H), 7.47 (d, J = 8.0 Hz, 1H), 7.27 (t, J = 8.0 Hz, 1H), 7.21 (t, J = 8.0 Hz, 1H), 7.05 (s, 1H), 6.81 (s, 8H). ^{13}C NMR (chloroform-d_1, 100 MHz): δ 156.2, 154.9, 147.0, 143.1, 141.7, 140.7, 138.8, 134.9, 129.8, 129.2, 128.2, 124.1, 122.8, 120.7, 111.3, 101.6, 23.4, 21.2. HRMS (MALDI, m/z): $[M+Na]^+$ calcd for $C_{50}H_{52}B_2O$, 713.4103; found, 713.4178. Anal Calcd for $C_{50}H_{52}B_2O$: C, 86.96; H, 7.59; B, 3.13. Found: C, 86.82; H, 7.56.

2.2.5. 10,10'-(5-Benzofuran-2-yl)-1,3-phenylene)bis(10H-phenothiazine) (*C-phOL*) and 10-(3- benzofuran-2-yl)-5-bromophenyl)-10H-phenothiazine (*1c*)

The flask loaded with **1b** (2.65 g, 7.53 mmol), phenothiazine (0.50 g, 2.51 mmol), sodium *tert*-botoxide (0.724 g, 7.53 mmol),

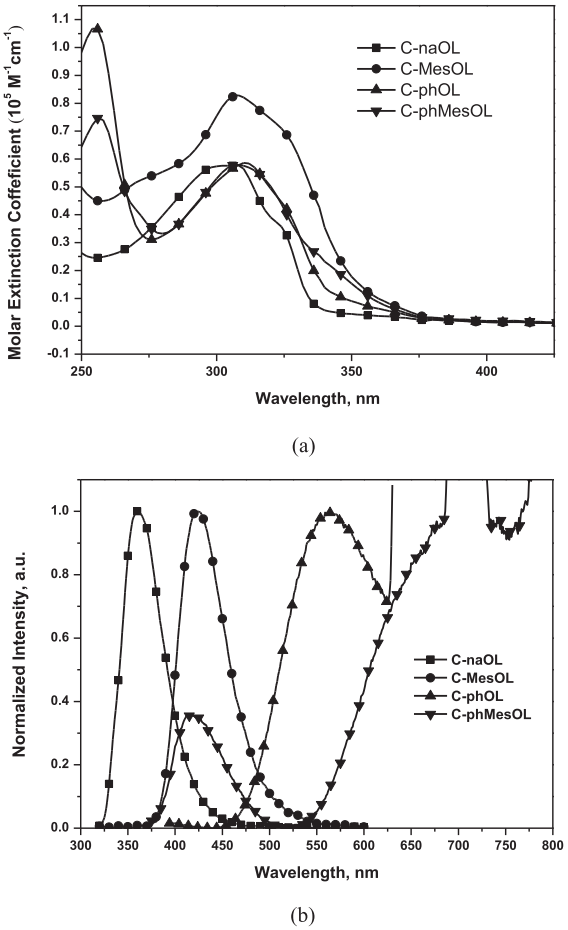

Fig. 2. Absorption (a) and emission spectra (b) of the compounds in CH_2Cl_2.

$Pd(dba)_2$ (0.057g, 0.10 mmol) was sequentially added toluene (25 mL) and tri(*tert*-butyl)phosphine (0.49 M in toluene, 0.41 mL, 0.20 mmol), and the solution was heated at 80 °C for 18 h. After removal of the solvent, the residue was dissolved in CH_2Cl_2 and filtered through Celite. The filtrate was extracted with CH_2Cl_2/saturated aqueous NH_4Cl for several times. The collected organic extracts were dehydrated by anhydrous $MgSO_4$ and filtered. The filtrate was pumped dry and the residue was further purified by column chromatography using CH_2Cl_2/hexanes (1:8 by vol.) as the eluent. The compound **1c** was isolated from the first band as a pale yellow powder in 28% yield (0.33g). ^{1}H NMR (acetone-d_6, 400 MHz): δ 8.15 (s, 1H), 7.91 (s, 1H), 7.67 (d, J = 7.6 Hz, 1H), 7.57 (m, 3H), 7.37 (m, 1H), 7.28 (m, 1H), 7.20 (d, J = 7.6 Hz, 2H), 7.09 (m, 2H), 7.00 (m, 2H), 6.65 (d, J = 8.4 Hz, 2H). ^{13}C NMR (acetone-d_6, 125 MHz): δ 156.0, 154.2, 145.3, 144.1, 135.6, 131.3, 129.9, 128.4, 128.2, 126.7, 126.3, 124.8, 124.4, 124.3, 123.8, 122.5, 119.7, 112.2, 105.0. HRMS (MALDI, m/z): $[M+H]^+$ calcd for $C_{26}H_{16}BrNOS$, 469.0136; found, 469.0151. The compound **C-phOL** was isolated from the second band as a yellow powder in 29% yield (0.34 g). ^{1}H NMR (acetone-d_6, 400 MHz): δ 8.00 (d, J = 2.0 Hz, 2H), 7.67 (d, J = 7.6 Hz, 1H), 7.57 (d, J = 8.4 Hz, 1H), 7.55 (s, 1H), 7.36 (m, 2H), 7.27 (m, 1H), 7.16 (dd, J = 7.6; 1.2 Hz, 4H), 7.07 (m, 4H), 6.96 (t, J = 7.6 Hz, 4H), 6.71 (d, J = 8.0 Hz, 4H). ^{13}C NMR (acetone-d_6, 125 MHz): δ 156.0, 155.0, 146.0, 144.5, 136.2, 130.1, 128.7, 128.4, 128.1, 126.2, 124.6, 124.4, 123.9, 123.7, 122.5, 119.3, 112.1, 104.6. HRMS (MALDI, m/z): $[M+H]^+$ calcd for $C_{38}H_{24}N_2OS_2$, 588.1330; found, 588.1340. Anal Calcd for $C_{38}H_{24}N_2OS_2$: C, 77.52; H, 4.11; N, 4.76; O, 2.72; S, 10.89. Found: C, 77.47; H, 4.28; N, 4.60.

2.2.6. 10-(3-Benzofuran-2-yl)-5-(dimesitylboryl)phenyl)-10H-phenothiazine (**C-phMesOL**)

To a flask containing **1c** (0.70 g, 84.6 mmol) in THF (85 mL) prechilled to −78 °C was added *n*-BuLi (2.5 M in hexane, 3.17 mL, 5.07 mmol) dropwise. After the solution was stirred for 45 min at the same temperature, a THF solution (15 mL) of dimesityl boron-fluoride (0.60 g, 2.24 mmol) was added. The solution was slowly warmed to room temperature at stirred for 18 h. The solution was quenched with de-ionized water and THF was removed by a rotatory evaporator. The solution was extracted with CH_2Cl_2/saturated aqueous NH_4Cl for several times. The collected organic extracts were dehydrated by anhydrous $MgSO_4$ and filtered. The filtrate was pumped dry and the residue was purified by column chromatography using hexanes as the eluent. The crude product obtained was recrystallized from CH_2Cl_2/cooled MeOH to provide the desired product as a yellow powder in 56% yield (0.53 g). ^{1}H NMR (acetone-d_6, 400 MHz): δ 8.17 (d, J = 4.0 Hz, 2H), 7.65 (d, J = 7.6 Hz, 1H), 7.55 (d, J = 8.0 Hz, 1H), 7.42 (s, 1H), 7.33 (m, 1H), 7.25 (m, 1H), 7.05 (d, J = 7.6 Hz, 2H), 6.94 (m, 2H), 6.86 (m, 6H), 6.33 (d, J = 8.0 Hz, 2H), 2.28 (s, 6H), 2.10 (s, 12H). ^{13}C NMR (acetone-d_6, 125 MHz): δ 155.9, 155.5, 151.7, 144.9, 142.7, 142.2, 141.6, 140.4, 138.4, 134.3, 131.8, 131.5, 130.0, 129.5, 128.0, 127.7, 125.9, 124.3, 123.8, 122.3, 121.0, 117.0, 112.0, 104.2, 23.9, 21.4. HRMS (MALDI, m/z): $[M+H]^+$ Calcd for $C_{44}H_{38}BNOS$, 639.2767; Found, 639.2782. Anal. Calcd for $C_{44}H_{38}BNOS$: C, 82.62; H, 5.99; B, 1.69; N, 2.19. Found: C, 82.73; H, 5.89; N, 2.48.

2.3. Quantum chemistry computation

The computation were performed with Q-Chem 4.0 software [11]. Geometry optimization of the molecules were performed using hybrid B3LYP functional and 6-31G* basis set. For each molecule, a number of possible conformations were examined and the one with the lowest energy was used. The same functional was also applied for the calculation of excited states using time-dependent density functional theory (TD−DFT). In the present work, we also use TD−DFT to visualize the extent of transition moments as well as their charge-transfer characters.

3. Results and discussion

3.1. Synthesis and thermal properties of the compounds

New 1,3,5-trisubstituted phenyl derivatives synthesized in this study are shown in Fig. 1. The synthetic route of the compounds is outlined in Scheme 1. Stille C−C coupling reaction [12] between 1,3,5-tribromobenzene and 1/3 equivalent of benzofuran-2-yltributylstannane (**1a**) provides **DBBF** (**1b**) in moderate yield. Compound **1b** then undergoes Suzuki C−C coupling reaction [13] with naphthalene-1-ylboronic acid to afford **C-naOL**. In contrast, Buchwald-Hartwig C−N coupling reaction [14] of **1b** with 1/3 equivalent of phenothiazine gives **1c** and **C-phOL** in nearly the same yield. Compounds **C-MeseOL** and **C-phMesOL** can be obtained from the reaction of dimesityl boronfluoride with lithiated **1b** and **1c**, respectively.

The thermal properties of the compounds were investigated by TGA (thermogravimetric analysis) and DSC (differential scanning calorimetry) measurements (Table 1). These compounds possess high thermal decomposition temperatures (T_d) ranging from 255 to 338 °C. Except for **C-phOL**, all the compounds readily form a glass from (T_g = 78−110 °C) their melts upon fast cooling and the glassy state persists in the subsequent heating cycles. Compared to other compounds, **C-naOL** has lower T_g and T_m values, possibly its lower molecular weight and less polar character lead to less intermolecular interaction.

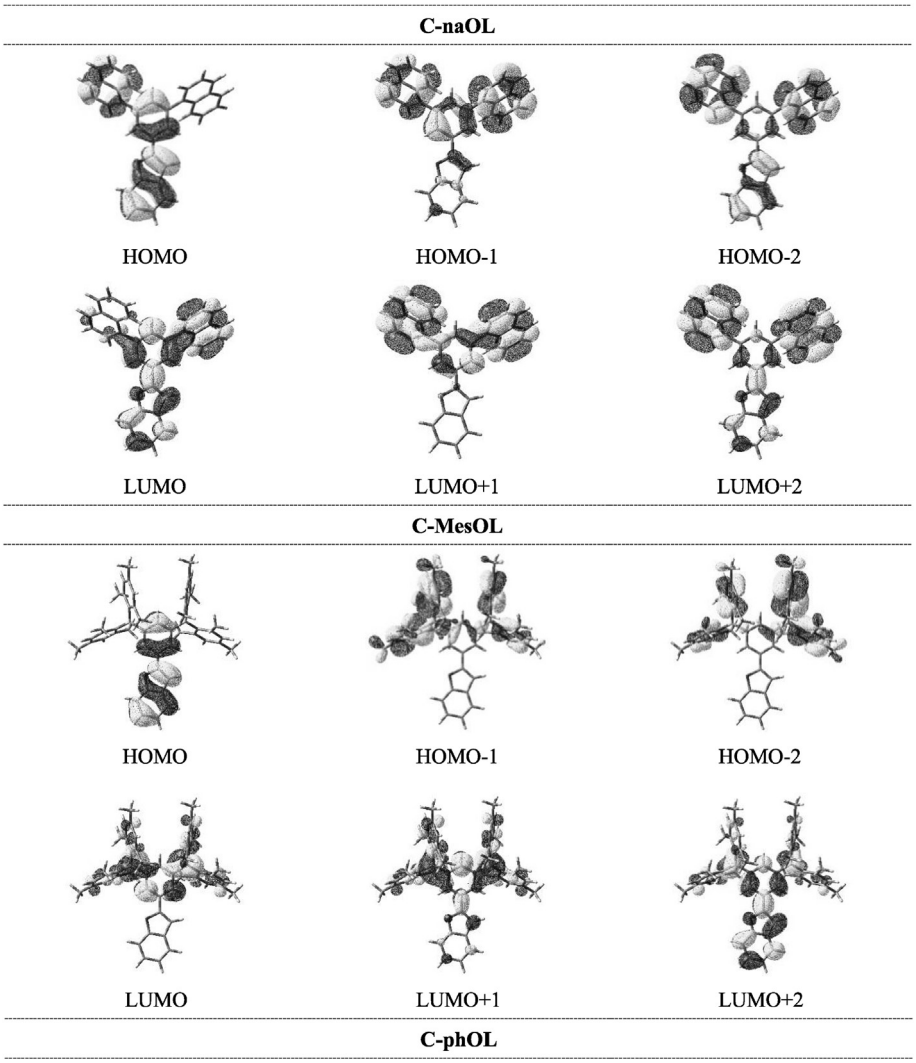

Fig. 3. Frontier orbitals of the compounds.

3.2. Photophysical properties

The absorption spectra of the compounds in CH_2Cl_2 are shown in Fig. 2. The band in the range of 275–350 nm is ascribed to the $\pi \rightarrow \pi^*$ transition and the λ_{abs} values are very similar among the compounds. The shoulder ranging from 325 to 375 nm is attributed to the intramolecular transfer transition (ICT) which is confirmed by theoretical computation (vide infra). Based on the computational results, the $S_0 \rightarrow S_n$ (n = 1–3) transitions of the molecules have very low intensity except for **C-naOL**. Some transition energies are also comparable for each compound. Consequently, estimation of the HOMO/LUMO gap from the absorption spectra is not unambiguous. We therefore estimate the HOMO/LUMO gap from the onset of the emission at the shorter wavelength side (**C-naOL**, 3.79 eV; **C-MesOL**, 3.24 eV; **C-phOL**, 2.57 eV; **C-phMesOL**, 2.22 eV: vide infra and Table 1) for our discussions. The wavelength of the ICT band normally increases with a stronger electron acceptor and donor. The order of decreasing ICT band wavelength (from both the emission spectra and theoretical computation), **C-phMesOL** > **C-MesOL** > **C-phOL** > **C-naOL**, is therefore in accordance with the order of the decreasing donor strength, phenothiazine > naphthyl > benzofuran, and the order of decreasing acceptor strength, dimesitylboryl > benzofuran > naphthyl. The emission spectra (Fig. 2b) of the compounds vary in both intensity and Stokes shift. Compounds **C-naOL** and **C-MesOL** have higher quantum yield (**C-naOL**: 0.80; **C-MesOL**: 0.33) and less Stokes shift as well as solvatochromic shift (THF vs. CH_2Cl_2) compared with the other two. This may be attributed to the more orbital overlap (vide infra, see computation) between the ground and excited state of **C-naOL** and **C-MesOL**. Energy gap law [15] may also accounts for the barely recognizable quantum yields of **C-phOL** and **C-phMesOL**. Compounds with arylamine and arylborane at the mutual *meta*-position of a phenylene linker were also reported to have low quantum yield [16]. Dual emission was also found in **C-phMesOL**. The emission at shorter wavelength (416 nm) is attributed to the $S_0 \rightarrow S_2$ transition which is originated from the benzofuran entity to the boran entity. This argument is supported by the PL spectrum of **C-phMesOL** film measured under excitation wavelength ranging from 260 to 330 nm (260, 275, 280, 290, 300, 310, and 330 nm). The emission at the shorter wavelength can be observed only when the excitation wavelength is shorter than 300 nm (the peak of the short-wavelength emission).

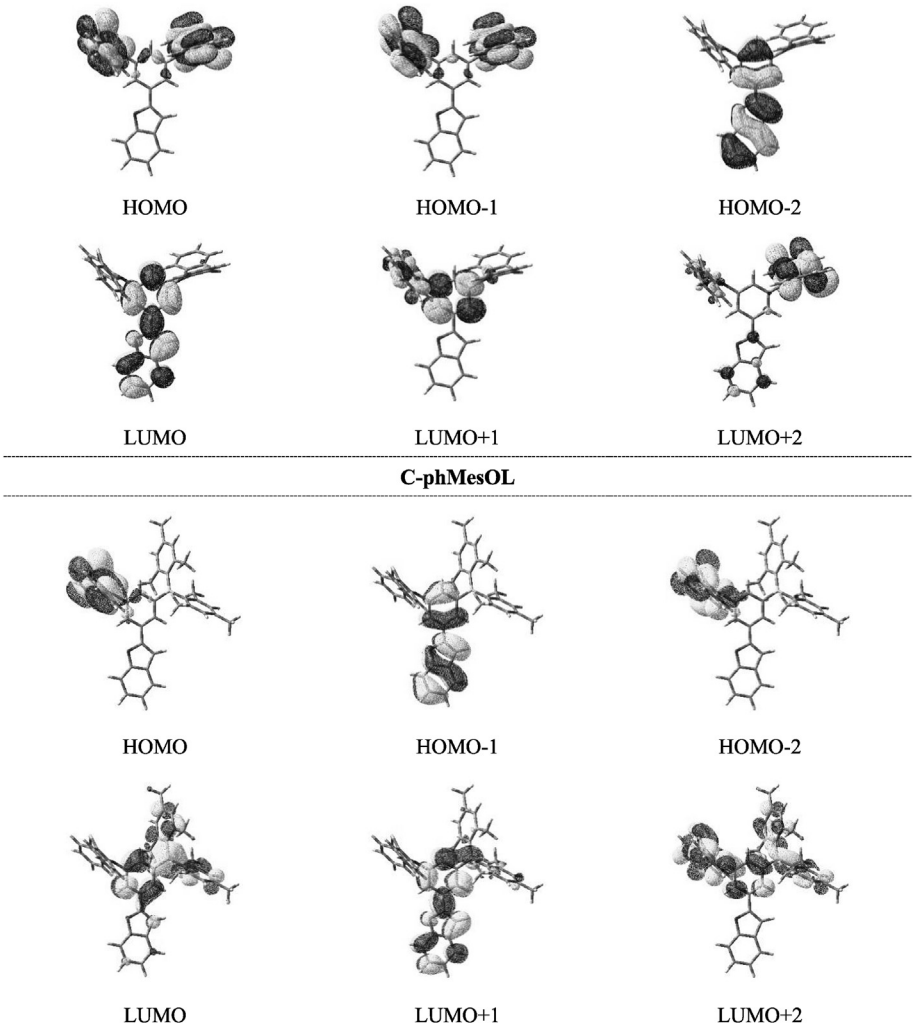

Fig. 3. (*continued*).

Table 2
Calculated lower-lying transitions of the dyes.[a]

dye	State	Excitation[b]	E_{cal}, eV	λ_{cal}, nm	*f*	Dye	State	excitation[b]	E_{cal}, eV	λ_{cal}, nm	*f*
C-naOL	S_1	H1 → L (39%) H → L (35%) H → L1 (20%)	3.78	329	0.08	C-MesOL	S_1	H → L (95%)	3.28	379	0.05
	S_2	H1 → L1 (12%) H1 → L (15%) H → L (50%) H → L1 (10%) H → L2 (6%)	3.94	315	0.24		S_2	H2 → L1 (6%) H1 → L1 (8%) H1 → L (81%)	3.54	351	0.09
	S_3	H1 → L (35%) H → L1 (62%)	3.95	315	0.17		S_3	H → L1 (91%) H → L2 (6%)	3.56	349	0.07
C-phOL	S_1	H → L (99%)	2.80	442	0.00	C-phMesOL	S_1	H → L (99%)	2.46	504	0.00
	S_2	H1 → L (99%)	2.90	429	0.00		S_2	H → L1 (98%)	3.05	407	0.00
	S_3	H1 → L1 (8%) H → L1 (89%)	3.40	365	0.00		S_3	H1 → L (96%)	3.33	373	0.06

[a] Results are based on gas-phase TD-DFT calculation.
[b] H = HOMO, L = LUMO, H1 = The next highest occupied molecular orbital, or HOMO − 1, H2 = HOMO − 2, L1 = LUMO +1, L2 = LUMO +2. In parentheses is the population of a pair of MO excitations.

3.3. Electrochemical properties

The electrochemical properties of the compounds were studied by cyclic voltammetric methods, and relevant data are shown in Table 1. Reversible oxidation waves were observed for **C-phOL** and **C-phMesOL** only, possibly due to the higher stability of the phenothiazine radical cation formed upon oxidation. While there is only one redox wave detected for **C-phMesOL** (352 mV vs. ferrocene/ferricenium) in THF, it is interesting that **C-phOL** exhibits two overlapping redox waves. However, the two redox waves can be

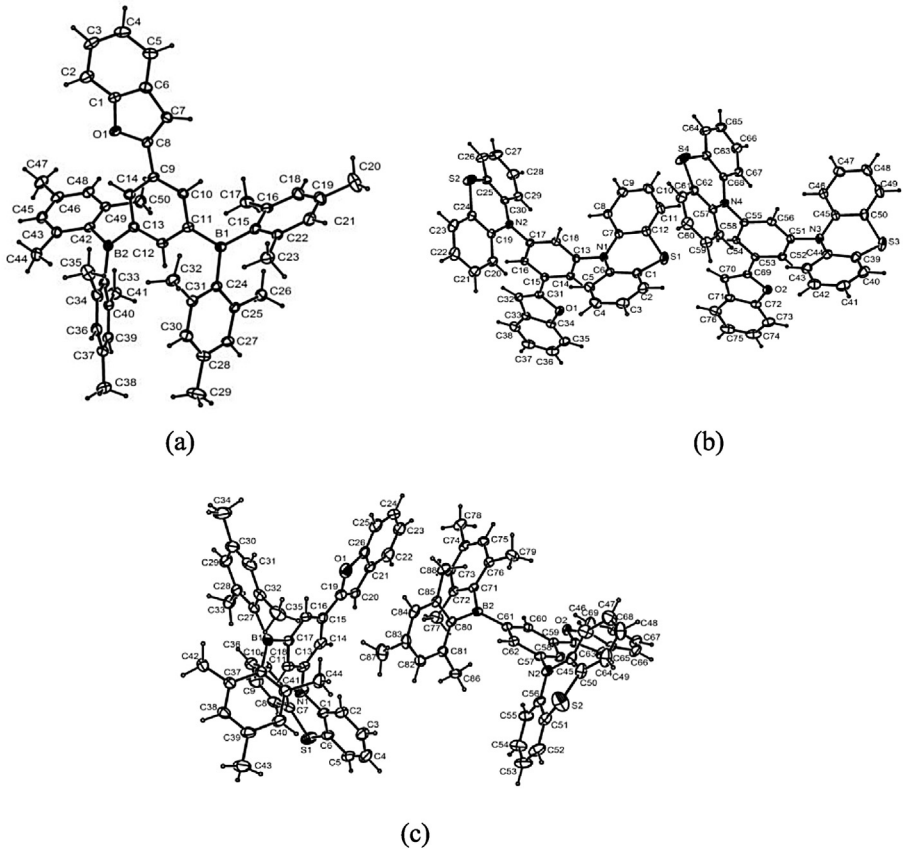

Fig. 4. X-ray structure of the compounds **C-MesOL** (a), **C-phOL** (b) and **C-phMesOL** (c).

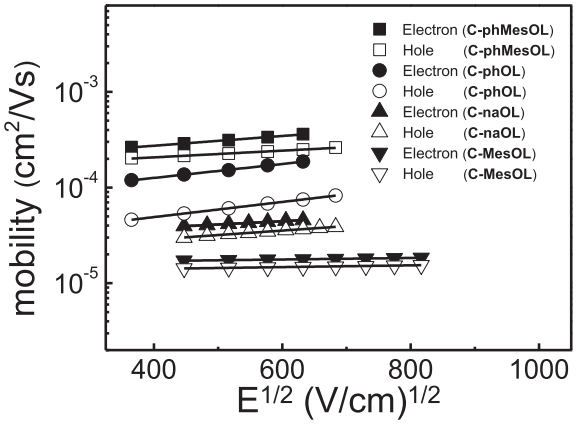

Fig. 5. Electron and hole mobilities versus $E^{1/2}$ for films of the compounds.

Table 3
Electron and hole mobilities of compounds measured from the time-of-flight method.

	μ_e[a] × 10^{-5} $cm^2/(V•s)$	μ_h[b] × 10^{-5} $cm^2/(V•s)$
C-naOL	4.6 (nd)	3.7 (nd)
C-MesOL	1.8 (d)	1.5 (d)
C-phOL	19 (nd)	7.5 (d)
C-phMesOL	36 (nd)	25 (d)

d: dispersive; nd: non-dispersive. The electric field applied: 4 × 10^5 V/cm.
[a] μ_e: electron mobility.
[b] μ_e: hole mobility.

completely resolved to two reversible redox waves (293 and 459 mV vs. ferrocene/ferricenium) in dichloromethane (Fig. S1). This phenomenum strongly suggests that there exists weak electronic interaction between the two phenothiazine entities in **C-phOL**. The ionization potentials of the compounds in the film state were measured using a low-energy photoelectron spectrometer (AC-2) (Fig. S2). These were then used to estimate the HOMO energy levels of the compounds (Table 1). The stronger donor normally leads to a high-lying HOMO level and a stronger acceptor results in a low-lying LUMO. Accordingly, **C-phOL** and **C-phMesOL** have upward shift of the HOMO level compared to the other two compounds. The trend of decreasing HOMO levels from AC2 measurement, **C-phOL** ≈ **C-phMesOL** > **C-naOL** > **C-MesOL**, is therefore in parallel with that observed from the CV data (vide supra). As the estimation of HOMO/LUMO gap from the absorption band edge or the intercept of the absorption and emission spectra is not trivial, we also list the HOMO and LUMO energies and the HOMO/LUMO gap ($E_{0\text{-}0}$) obtained from the computation in Table 1 for reference.

3.4. Theoretical computation

Quantum chemistry computation was carried out on the compounds in this study. The computed frontier orbitals of the compounds and their corresponding energy states are included in Fig. 3, and the results for theoretical computation are listed in Table 2. The $S_0 \rightarrow S_1$ transition of **C-naOL** has more prominent $\pi \rightarrow \pi^*$ character. In contrast, the $S_0 \rightarrow S_1$ transitions of the other three have prominent ICT character: from benzofuran entity to boran entity in **C-MesOL**, from phenothiazine entity to benzofuran entity in **C-phOL** and from naphthylene entity to boran entity in **C-phMesOL**,

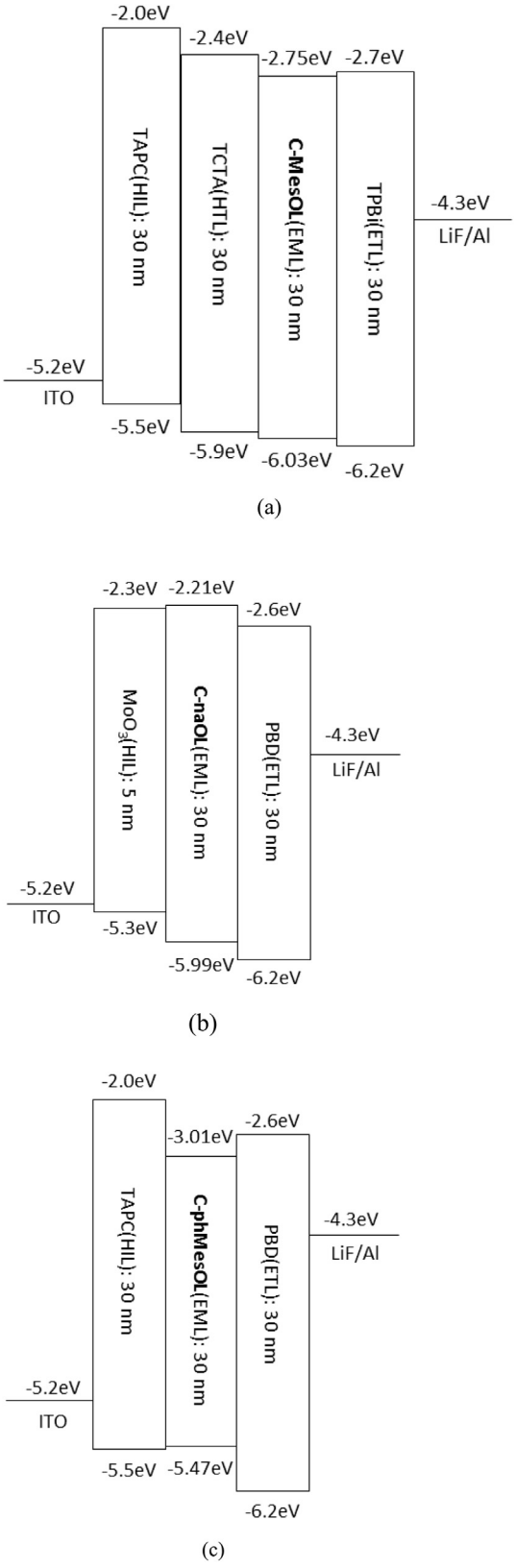

Fig. 6. Relative energy alignments in the OLED device: (a) device I, (b) device II, and (c) device III.

respectively. However, the ICT bands have very low oscillator strengths because of the mutual *meta*-orientation of the donor and the acceptor. The energy of the $S_0 \rightarrow S_1$ transition increases in the order of **C-phMesOL** < **C-MesOL** < **C-phOL** < **C-naOL**, which is in parallel with the trend of the emission spectra, though the absorption spectra do not account for the conformational relaxation of the Frank Condon excited state.

3.5. Crystal structures

Single crystals suitable for X-ray diffraction analysis were obtained by slow diffusion of methanol (**C-MesOL** and **C-phOL**) or hexane (**C-phMesOL**) to the dichloromethane solutions of the corresponding complex, respectively. ORTEP plots are displayed in Fig. 4. Selected bond distances and bond angles are collected in Table S1. The bond distances and angles appear to be normal. Two independent molecules exist in the same unit cell for both **C-phOL** and **C-phMesOL**, and the two independent molecules have similar conformation except for the dihedral angles between the two phenyl rings belonging to the same phenothiazine unit due to nonplanar nature of the phenothiazine. In **C-phOL**, the dihedral angles are 31.21 and 7.14° for one and 26.44 and 16.94° for the second molecule, respectively. In **C-phMesOL**, the dihedral angles for the two molecules are 22.80 and 9.16°, respectively. There is large twist angle between the central phenyl ring and the phenothiazine segment (the best plane formed from the nitrogen atom and the three ipso carbons of the neighboring phenyl rings) for both **C-phOL** (85.91 and 86.49° for one molecule; 86.45 and 87.24° for the other molecule) and **C-phMesOL** (80.28 and 83.72°). The twist angle between the benzofuran and the central phenyl ring is small for all the compounds: **C-phOL**, 2.01 and 8.14°; **C-MesOL**, 10.21°; **C-phMesOL**, 5.48 and 5.64°. The boron atom is coplanar with the ipso carbon atoms from the three neighboring phenyl rings, and the mesityl rings are twisted from this plane by 75.93 and 71.67° for one molecule and 75.63 and 66.43° for the other molecule in the lattice of **C-phMesOL**, and by 73.06 and 67.42° for one bororyl unit and 68.14 and 70.83° for the other bororyl unit in the lattice of **C-MesOL**. Among the crystal lattices of the three compounds, π–π interaction was found only in **C-MesOL**. Each molecule forms weak π–π interaction (with a distance of 3.948 Å) with one neighboring molecule via the benzofuran entity. However, such close contact exists only in pairs of molecules and no infinite linkage can be found. Therefore, no solid clue on the carrier mobility (vide infra) can be retrieved from the crystal structural analysis.

3.6. Charge-transport properties

The carrier-transport properties of the compounds were investigated by the time-of-flight (TOF) transient-photocurrent technique at room temperature [17]. The representative TOF transients for electrons and holes of the compounds are shown in Fig. S3 (Supporting Information), and the intersection point of two asymptotes in the double logarithmic representation of these plots are used to calculate the carrier mobilities. All of the compounds exhibit ambipolar carrier-transport behavior, with either dispersive or non-dispersive carrier-transport characteristics. Fig. 5 shows the dependence of the carrier mobilities of various compounds on the electric filed, and the carrier mobilities at the electric field of 4×10^5 V/cm are given in Table 3. The field dependence of carrier mobilities follows the nearly universal Poole-Frenkel relationship: $\mu \propto \exp(\beta E^{1/2})$, where β is the Poole–Frenkel factor [18]. Both hole and electron mobilities of the compounds are in the range of 10^{-4}–10^{-5} $cm^2/(V\ s)$. The hole mobilities are slightly lower than those (~10^{-3} $cm^2/V\ s$) of commonly used diphenylamino-based hole-transport materials, *N,N′*-di(1-naphthyl)-*N,N′*-diphenyl-(1,1′-biphenyl)-4,4′-diamine (NPB) [19a] and *N,N*'-diphenylbenzidine (TPD) [19b]. In contrast, the electron mobilities of the compounds

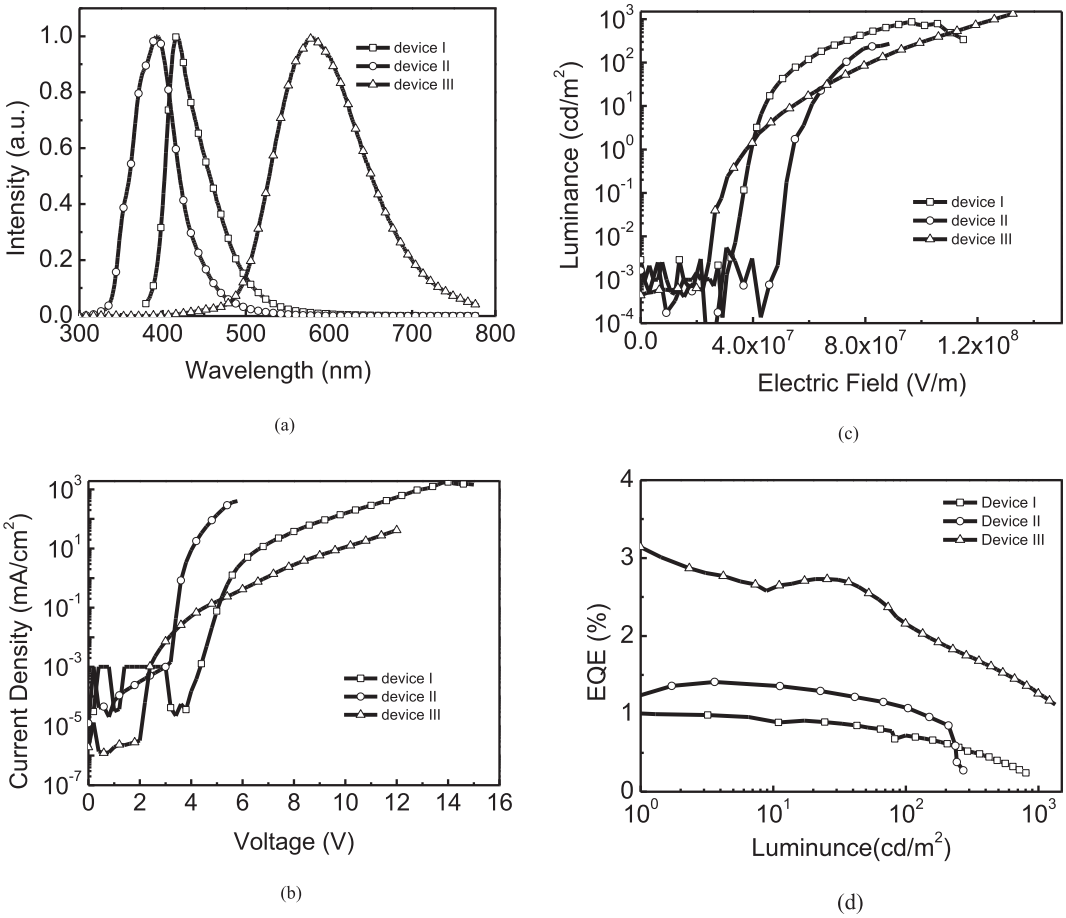

Fig. 7. (a) EL spectra, (b) *I*–*V* plot, (c) luminance vs. applied electric field and (d) EQE of the OLED devices.

Table 4
Electroluminescent data of the device.[a]

	C-MesOL	C-naOL	C-phMesOL
*V*on, V	5.1	3.51	3.4
L_{max}, cd/m^2 (voltage, V)	8719 (12.6);	256 (5.8)	1340 (12)
λ_{em}, nm	416	393	579
CIE (x,y)	(0.1576, 0.0661)	(0.1601, 0.0428)	(0.482, 0.491)
fwhm, nm	56	58	124
$\eta_{ext,max}$, %	1.01	1.41	3.14
$\eta_{p,max}$, lm/W	0.33	0.22	5.19
$\eta_{c,max}$, cd/A	0.55	0.25	7.36
η_{ext}, %[b]	0.40	1.08	1.26
η_p, lm/W[b]	0.22	0.08	0.99
η_c, cd/A[b]	0.64	0.12	3.61

[a] L_{max}, maximum luminance; V_{on}, turn-on voltage; *V*, voltage; λ_{em}, emission wavelength; CIE (x,y), Commission Internationale de l'Eclairage coordinates; fwhm, full width at half maximum; $\eta_{ext,max}$, maximum external quantum efficiency; $\eta_{p,max}$, maximum power efficiency; $\eta_{c,max}$, maximum current efficiency; *L*, luminance; η_{ext}, *external quantum efficiency;* η_p, power efficiency; η_c, current efficiency.

[b] At a current density of 500 (device I), 100 (device II) or 1000 (device III) cd/m^2. V_{on} was obtained from the x-intercept of log(luminance) vs. applied voltage plot.

are slightly better than those of the typical electron-transport materials, TPBI (~10^{-5} cm^2/(V s)) [20a] and *N*-arylbenzimidazole-containing analogues (~10^{-5}–10^{-6} cm^2/(V s)) [20b]. All the compounds exhibit comparable electron and hole mobilities, and **C-phMesOL** containing potent ET (dimesitylborane) and HT (phenothiazine) entities has the highest carrier mobilities among all.

3.7. Electroluminescent properties

Among four compounds, **C-naOL** and **C-MesOL** are emissive with quantum yields of ~100% and 33%, respectively. Due to low glass transition temperature (T_g) of **C-naOL** (78 °C), only **C-MesOL** was subjected to OLED fabrication. After careful analysis of the HOMO and LUMO energies for the compounds and some relatively available injection/transport materials (Fig. 6), the OLEDs with different configurations were fabricated: device I: ITO (120 nm)/TAPC (30 nm)/TCTA (40 nm)/**C-MesOL** (30 nm)/TPBi (30 nm)/LiF (0.5 nm)/Al (130 nm) was fabricated, where TAPC (1,1-bis((di-4-tolylamino)phenyl)cyclohexane)), TCTA (4,4′,4″-tris(*N*-carbonyl) triphenylamine) and TPBI (1,3,5- tris(*N*-phenylbenzimidazol-2-yl)-benzene) were the hole injection, hole transport and electron transport materials, respectively; device II: ITO (120 nm)/MoO_3 (5 nm)/**C-naOL** (30 nm)/PBD (30 nm)/LiF (0.5 nm)/Al (130 nm), where MoO_3 and PBD (2-(4-biphenyl)-5-(4-*tert*-butylphenyl)-1,3,4-oxadiazole) were used as the hole injection and electron transport material; device III: ITO (120 nm)/TAPC (30 nm)/**C-phMesOL** (30 nm)/PBD (30 nm)/LiF (0.5 nm)/Al (130 nm), where TAPC and PBD were used as the hole injection and electron transport materials, respectively. The EL spectrum, *I*–*V*-*L* characteristic and efficiency plots are shown in Fig. 7, and the performance parameters are compiled in Table 4. The devices I emits violet light, and the EL spectrum bears close resemblance to the PL spectrum, indicating that light emission is originated from the emitting layer. The device II also emits violet light, and the EL spectrum is slightly red shifted, which may be due to microcavity effect. The

performance for the two devices is only mediocre. The non-optimized device exhibited the following performance parameters: I, $\eta_{ext,max}$ = 1.01% at 1 cd/m^2, $\eta_{p,max}$ = 0.22 lm/W, $\eta_{c,max}$ = 0.55 cd/A, λ_{max} = 416 nm; V_{on} = 5.1 V, L_{max} = 8719 cd/m^2; II, $\eta_{ext,max}$ = 1.41% at 1 cd/m^2, $\eta_{p,max}$ = 0.22 lm/W, $\eta_{c,max}$ = 0.25 cd/A, λ_{max} = 393 nm, V_{on} = 3.51 V, L_{max} = 256 cd/m^2. The device III emits yellow-orange light, and the EL spectrum is similar to the PL spectrum at the longer wavelength region. The absence of the shorter wavelength emission in the EL spectrum ($S_2 \rightarrow S_0$ transition, vide supra) may be due to unavailability of the high-lying LUMO+1 orbital at the applied potential. The external quantum efficiency reaches 3.14% despite of very low solution quantum yield of **C-phMesOL**. Possibly there exists aggregation enhanced emission [21] at the longer wavelength region. Use of **C-phMesOL** as the host for phosphorescent Ir complex, Ir(pq)$_2$(acac) [22], was also tested. However, the EL spectrum was the same as that of non-doped device, likely due to inefficient energy transfer between **C-phMesOL** and Ir(pq)$_2$(acac).

In addition to full-color light-emitting displays, OLEDs with shorter wavelength emission including UV, violet and deep blue, have potential applications in biological and chemical sensing [23] and information storage [24]. The device performance of the two violet emitting OLEDs in this study appear to be comparable with that reported for dipolar purine dye [25] and substituted phenylsilane [26] dye. Though the excitons were successfully confined in the emitting layer in both devices, future endeavor includes improving the performance and the long-term stability of the device.

4. Conclusions

In summary, bipolar transport materials were successfully synthesized using a phenyl core with *meta*-substituted benzofuranyl and naphthyl (or phenothiazinyl, dimesitylbpryl and phenathiazine and dimesitylboryl) entities. The compounds have hole mobility and electron mobility in the range of 1.8–36 and 1.5–2.5 $\times$ 10^{-5} cm^2/V•s, respectively. Two violet-emitting compounds of good quantum yield were fabricated as violet-emitting OLED, and the external quantum efficiencies reached 1.01% and 1.41%, respectively. A yellow-orange OLED with an efficiency of 3.14% was also fabricated.

Acknowledgments

Financial support of this research by Academia Sinica (AS) and Ministry of Science and Technology (MOST, Taiwan) (MOST 104-2113-M-001-009-MY3) are gratefully acknowledged. Support from the Instrumentation Center of Institute of Chemistry (AS) and National Taiwan Normal University (NTNU) is also acknowledged.

Appendix A. Supplementary data

Supplementary data related to this article can be found at http://dx.doi.org/10.1016/j.orgel.2015.12.026.

References

[1] a) S. Karabunarliev, M. Baumgarten, N. Tyutyulkov, K. Müllen, J. Phys. Chem. 98 (1994) 11892;
b) S.Y. Hong, D.Y. Kim, C.Y. Kim, R. Hoffmann, Macromolecules 34 (2010) 6474.
[2] a) K.M. Gaab, A.L. Thompson, J. Xu, T.J. Martinez, C.J. Bardeen, J. Am. Chem. Soc. 125 (2003) 9288;
b) A.L. Thompson, K.M. Gaab, J. Xu, C.J. Bardeen, T.J. Martinez, J. Phys. Chem. 108 (2004) 671.
[3] A. Chaskar, H.-F. Chen, K.-T. Wong, Adv. Mater. 23 (2011) 3876.
[4] a) M.-Y. Lai, C.-H. Chen, W.-S. Huang, J.T. Lin, T.-H. Ke, L.-Y. Chen, M.-H. Tsai, C.-C. Wu, Angew. Chem. Int. Ed. 47 (2008) 581;
b) C.-H. Chen, W.-S. Huang, M.-Y. Lai, W.-C. Tsao, J.T. Lin, Y.-H. Wu, T.-H. Ke, L.-Y. Chen, M.-H. Tsai, C.-C. Wu, Adv. Funct. Mater. 19 (2009) 2661.
[5] a) S. Anderson, P.N. Taylor, G.L.B. Verschoor, Chem. Eur. J. 10 (2004) 518;
b) N.G. Kundu, M. Pal, J.S. Mahanty, M. De, J. Chem. Soc. Perkin Trans. 1 (1) (1997) 2815;
c) J.R. Hwu, K.-S. Chuang, S.H. Chuang, S.-C. Tsay, Org. Lett. 7 (2005) 1545.
[6] G. Valchanov, A. Ivanova, A. Tadjer, D. Chercka, M. Baumgarten, Org. Electron. 14 (2013) 2727.
[7] C.D. Entwistle, T.B. Marder, Chem. Mater. 16 (2004) 4574.
[8] a) T. Noda, H. Ogawa, N. Noma, Y. Shirota, J. Mater. Chem. 9 (1999) 2177;
b) Y. Shirota, J. Mater. Chem. 15 (2005) 79.
[9] a) C.H. Zhao, A. Wakamiya, Y. Inukai, S. Yamaguchi, J. Am. Chem. Soc. 128 (2006) 15934;
b) S.L. Lin, L.H. Chan, R.H. Lee, M.Y. Yen, W.J. Kuo, C.T. Chen, R. Jeng, J. Adv. Mater. 20 (2008) 3947.
[10] a) J.N. Demas, G.A. Crosby, J. Phys. Chem. 75 (1971) 991;
b) W. Yan, Q. Wang, Q. Lin, M. Li, J.L. Petersen, X. Shi, Chem. Eur. J. 17 (2011) 5011.
[11] Y. Shao, L. Fusti-Molnar, Y. Jung, J. Kussmann, C. Ochsenfeld, S.T. Brown, A.T.B. Gilbert, L.V. Slipchenko, S.V. Levchenko, D.P. O'Neill, R.A. DiStasio Jr., R.C. Lochan, T. Wang, G.J.O. Beran, N.A. Besley, J.M. Herbert, C.Y. Lin, T. Van-Voorhis, S.H. Chien, A. Sodt, R.P. Steele, V.A. Rassolov, P.E. Maslen, P.P. Korambath, R.D. Adamson, B. Austin, J. Baker, E.F.C. Byrd, H. Dachsel, R.J. Doerksen, A. Dreuw, B.D. Dunietz, A.D. Dutoi, T.R. Furlani, S.R. Gwaltney, A. Heyden, S. Hirata, C.-P. Hsu, G. Kedziora, R.Z. Khaliullin, P. Klunzinger, A.M. Lee, M.S. Lee, W. Liang, I. Lotan, N. Nair, B. Peters, E.I. Proynov, P.A. Pieniazek, Y.M. Rhee, J. Ritchie, E. Rosta, C.D. Sherrill, A.C. Simmonett, J.E. Subotnik, H.L. Woodcock III, W. Zhang, A.T. Bell, A.K. Chakraborty, D.M. Chipman, F.J. Keil, A. Warshel, W.J. Hehre, H.F. Schaefer III, J. Kong, A.I. Krylov, P.M.W. Gill, M. Head-Gordon, Z. Gan, Y. Zhao, N.E. Schultz, D. Truhlar, E. Epifanovsky, M. Oana, R. Baer, B.R. Brooks, D. Casanova, J.-D. Chai, C.-L. Cheng, C. Cramer, D. Crittenden, A. Ghysels, G. Hawkins, E.G. Hohenstein, C. Kelley, W. Kurlancheek, D. Liotard, E. Livshits, P. Manohar, A. Marenich, D. Neuhauser, R. Olson, M.A. Rohrdanz, K.S. Thanthiriwatte, A.J.W. Thom, V. Vanovschi, C.F. Williams, Q. Wu, Z.-Q. You, E. Sundstrom, J. Parkhill, K. Lawler, D. Lambrecht, M. Goldey, R. Olivares-Amaya, Y. Bernard, L. Vogt, M. Watson, J. Liu, S. Yeganeh, B. Kaduk, O. Vydrov, X. Xu, I.A. Kaliman, C. Zhang, N. Russ, I.Y. Zhang, W.A. Goddard III, N. Besley, A. Ghysels, A. Landau, M. Wormit, A. Dreuw, M. Diedenhofen, A. Klamt, A.W. Lange, D. Ghosh, D. Kosenkov, A. Landou, D. Zuev, J. Deng, S.P. Mao, Y.C. Su, D. Small, Q-chem, Version 4.0, Q-Chem Inc, Pittsburgh, PA, 2011.
[12] J.K. Stille, Angew. Chem. Int. Ed. Engl. 25 (1986) 508.
[13] A. Suzuki, J. Organomet. Chem. 576 (1999) 147.
[14] A.S. Guram, R.A. Rennels, S.L. Buchwald, Angew. Chem. Int. Ed. 34 (1995) 1348.
[15] J.V. Caspar, T.J. Meyer, J. Phys. Chem. 87 (1983) 952.
[16] A.G. Bonn, O.S. Wenger, J. Org. Chem. 80 (2015) 4097.
[17] a) C.-C. Wu, T.-L. Liu, W.-Y. Hung, Y.-T. Lin, K.-T. Wong, E.-T. Chen, Y.-M. Chen, Y.-Y. Chien, J. Am. Chem. Soc. 125 (2003) 3710;
b) L.-Y. Chen, W.-Y. Hung, Y.-T. Lin, C.-C. Wu, T.-C. Chao, T.-H. Hung, K.-T. Wong, Appl. Phys. Lett. 87 (2005) 112103;
c) C.-C. Wu, W.-Y. Hung, T.-L. Liu, L.-Z. Zhang, T.-Y. Luh, J. Appl. Phys. 93 (2003) 5465.
[18] W.D. Gill, J. Appl. Phys. 43 (1972) 5033.
[19] a) L.-B. Lin, R.H. Young, M.G. Mason, S.A. Jenekhe, P.M. Borsenberger, Appl. Phys. Lett. 72 (1998) 864;
b) S. Naka, H. Onnagawa, Y. Yamaguchi, T. Tsutsui, Synth. Met. 111–112 (2000) 331.
[20] a) Y.Q. Li, M.K. Fung, Z. Xie, S.-T. Lee, L.-S. Hung, J. Shi, Adv. Mater. 14 (2002) 1317;
b) T.C. Wong, J. Kovac, C.S. Lee, L.S. Hung, S.T. Lee, Chem. Phys. Lett. 334 (2001) 61.
[21] Y. Hong, J.W.Y. Lam, B.Z. Tang, Chem. Commun. (2009) 4332.
[22] S. Lamansky, P. Djudovich, D. Murphy, F. Abdel-Razaq, R. Kwong, I. Tsyba, M. Bortz, B. Mui, R. Bau, M.E. Thompson, Inorg. Chem. 40 (2001) 1704.
[23] a) J. Shinar, R. Shinar, J. Phys. D. Appl. Phys. 41 (2008) 133001;
b) S. Landgraf, J. Biochem. Biophys. Methods 61 (2004) 125.
[24] H. van Santen, J.H.M. Neijzen, Jpn. J. Appl. Phys. 42 (2003) 1110.
[25] Y. Yang, P. Cohn, S.-H. Eom, K.A. Abbound, R.K. Castellano, J. Xue, J. Mater. Chem. C 1 (2013) 2867.
[26] X. Tang, L. Yao, H. Liu, F. Shen, S. Zhang, Y. Zhang, H. Zhang, P. Lu, Y. Ma, J. Mater. Chem. C 2 (2014) 5019.